

Single-site magnetic anisotropy governed by inter-layer cation charge imbalance in triangular-lattice AYbX_2

Ziba Zangeneh,¹ Stanislav Avdoshenko,¹ Jeroen van den Brink,^{1,2} and Liviu Hozoi¹

¹*Leibniz-Institute for Solid State and Materials Research,
IFW Dresden, Helmholtzstr. 20, 01069 Dresden, Germany*

²*Department of Physics, Technical University Dresden, Helmholtzstr. 10, 01069 Dresden, Germany*
(Dated: September 4, 2019)

The behavior in magnetic field of a paramagnetic center is characterized by its g tensor. An anisotropic form of the latter implies different kind of response along different crystallographic directions. Here we shed light on the anisotropy of the g tensor of $\text{Yb}^{3+} 4f^{13}$ ions in NaYbS_2 and NaYbO_2 , layered triangular-lattice materials suggested to host spin-liquid ground states. Using quantum chemical calculations we show that, even if the ligand-cage trigonal distortions are significant in these compounds, the crucial role in realizing strongly anisotropic, “noncubic” g factors is played by inter-layer cation charge imbalance effects. The latter refer to the asymmetry experienced by a given Yb center due to having higher ionic charges at adjacent metal sites within the magnetic ab layer, i.e., 3+ nearest neighbors within the ab plane versus 1+ species between the magnetic layers. According to our results, this should be a rather general feature of $4f^{13}$ layered compounds: less inter-layer positive charge is associated with stronger in-plane magnetic response.

Introduction

Certain features of the magnetic interactions in Mott-Hubbard insulators may be anticipated already on the basis of details of their crystal structure. For example, for weak spin-orbit coupling (SOC), edge-sharing ligand and octahedra with metal-ligand-metal bond angles close to 90° are usually associated with ferromagnetic (FM) Heisenberg exchange while corner-sharing ligand octahedra (i.e., metal-ligand-metal bond angles of 180° or somewhat less than 180° when distortions are present) give rise to antiferromagnetic (AF) interactions. This trend is materialized in two of the Goodenough-Kanamori-Anderson rules for magnetic interactions in transition-metal oxides and halides [1–5].

Another structural detail that can affect the valence energy levels and magnetic couplings is the presence of large differences between cation charges in ternary and quaternary compounds. It turns out that charge ‘asymmetry’ within the cation sublattice leads for instance to surprisingly large transition-metal t_{2g} - e_g gaps in certain double perovskites [6] and to an anomalous sequence of the t_{2g} levels and anomalous g factors in layered square-lattice materials [7]. The precise charge and position of cation species in-between the magnetically active layers also strongly affect the strength of both isotropic and anisotropic intersite exchange couplings [8, 9]. Further, the interplay between cation charge imbalance in the immediate surroundings and distortions of the ligand cage allows in principle tuning of the single-ion anisotropy [10].

While such effects have been addressed so far in transition-metal compounds, much less is known in this regard in the context of correlated f -electron systems. The f orbitals being much tighter, it is not *a priori* clear if the asymmetry of the cation charge distribution in the nearby surroundings significantly affects f -shell states as

well. Here we address such physics in the case of the $4f^{13}$ delafossites NaYbS_2 and NaYbO_2 , layered triangular-lattice materials suggested recently to host spin-liquid ground states [11–15]. We employ to this end quantum chemical calculations and reveal significant effects of this type on the f -level electronic structure. In particular, we find that, even if the trigonal distortions of the ligand cages are sizable in these compounds, the crucial role in realizing strongly anisotropic, noncubic g factors is played by inter-layer cation charge imbalance. The latter competes with the effect of trigonal compression of the ligand octahedra, is strong enough to substantially modify the f -level splittings, and this way gives rise to highly anisotropic g factors. Consequently, less inter-layer positive charge is associated with stronger in-plane magnetic response, a result that should be a rather general feature in $4f^{13}$ layered compounds, intensively investigated nowadays as possible platforms for spin-liquid phases.

Material model, computational scheme

The discovery of the triangular-lattice magnet YbMgGaO_4 as a promising spin-liquid candidate [16–21] has generated further interest in the search for Yb-based systems with similar properties. Recently the ternary Yb-based delafossite-type compounds with the formula AYbX_2 ($A = \text{Na}$ and $X = \text{S}, \text{O}$) have gained a lot of attention in this context [11–15]. Trigonal distorted YbX_6 octahedra share edges in these materials to form a two-dimensional triangular magnetic lattice of Yb^{3+} ions. Successive layers are stacked along the crystallographic c axis and separated by non-magnetic Na^+ species (see Fig. 1(a)). To describe the f -level electronic structure of Yb^{3+} ions in this type of crystalline environment, we performed *ab initio* quantum chemical embedded-cluster cal-

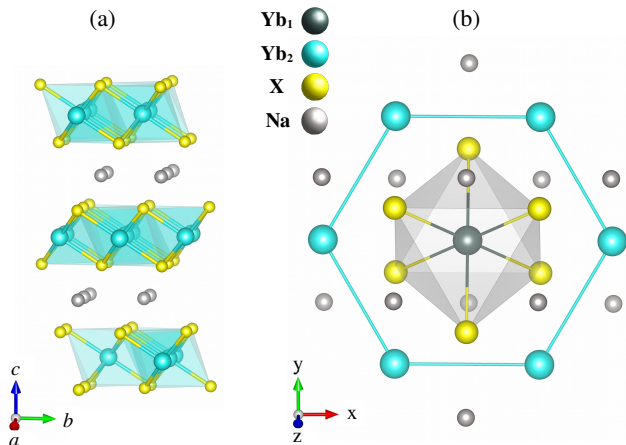


FIG. 1. Crystal structure of NaYbX₂: (a) Stacking of YbX₂ triangular layers on top of each other. (b) The reference YbX₆ octahedron, the six NN Yb atoms, and the adjacent Na ions explicitly included in the calculations. As our study is focused on single-site properties (Yb₁ central site), the adjacent six Yb ions (Yb₂) enter the calculations as large-core pseudopotentials [22] that include as well the f electrons (see text for more details). The extended solid-state surroundings were modeled as an effective embedding potential.

culations. For this purpose, we used a finite atomic fragment as shown in Fig. 1(b), which consists of one YbX₆ reference octahedron, the six nearest-neighbor (NN) Yb atoms, and the first Na-ion coordination shell. The remaining part of the crystalline lattice was modeled as a large array of point charges fitted to reproduce the crystal Madelung field in the cluster region. The point-group symmetry is here D_{3d} .

All quantum chemical calculations were performed with the MOLPRO package [23]. For the initial complete-active-space self-consistent-field (CASSCF) optimization [24], we considered all seven f orbitals at the central Yb site in the active space. Subsequently, the Yb $4f$ and S $3s$, $3p$ (or O $2s$, $2p$) electrons belonging to the central octahedron were correlated in multireference configuration interaction (MRCI) [24] computations with single and double excitations. The reference CASSCF wavefunctions were optimized for all seven possible states associated with the $4f^{13}$ manifold. All these eigenvectors entered the spin-orbit (SO) calculations, in both CASSCF and MRCI. For the central Yb ion we employed energy-consistent relativistic pseudopotentials [25] and Gaussian-type valence basis functions of quadruple-zeta quality [26, 27] while for the ligands of the central YbX₆ octahedron we applied all-electron valence triple-zeta basis sets [28, 29]. The occupied shells of the Na ions were described as large-core pseudopotentials from the MOLPRO library [30]. To obtain a clear picture on

crystal-field (CF) effects and SO interactions at the central Yb site, we cut off the magnetic couplings with the adjacent six Yb ions by applying large-core pseudopotentials that also incorporate the $4f$ electrons [22].

Basic electronic structure

Results for the f -level electronic structure are provided for NaYbS₂ and NaYbO₂ in Table I and Table II, using crystallographic data as reported in Refs. 31 and 32, respectively. Yb³⁺ $4f^{13}$ CF splittings were first obtained by CASSCF and MRCI calculations without SOC. Given the D_{3d} point-group symmetry, the seven f levels split into two groups of doubly degenerate E_u and three non-degenerate A_{2u} ($\times 2$) and A_{1u} ($\times 1$) components [33]. Without SO interactions we find the ${}^2A_{2u}$ state to be the lowest in energy for both NaYbS₂ and NaYbO₂ but our results indicate significantly larger CF splittings for the latter. This can be attributed to having shorter Yb-X distances (2.24 vs. 2.71 Å) and larger X-Yb-X angles (i.e., stronger trigonal compression, 96.3° vs. 92.2° X-Yb-X angles for ligands on the same side of the honeycomb plane) in NaYbO₂ as compared to NaYbS₂.

Results of SO-CASSCF and SO-MRCI calculations are listed for NaYbS₂ and NaYbO₂ in Table II. The SO calculations were performed according to the methodology described in Ref. 34, using Davidson-corrected [24] MRCI energies as diagonal elements in the SO matrix.

Just as for a free f^{13} ion, there is a large separation of more than 1 eV between the lowest four Kramers doublets (${}^2F_{7/2}$ term in the case of the free ion) and the higher-lying states (${}^2F_{5/2}$ term) [35]. In NaYbS₂, SO-MRCI puts the low-lying excited states at 15, 23, and 39 meV with respect to the ground-state Kramers doublet. Higher excitation energies of 39, 46, and 92 meV

TABLE I. CASSCF and MRCI results for the f -shell single-hole levels sans SOC in NaYbS₂ and NaYbO₂. Units of meV are used. In D_{3d} point-group symmetry, the f levels split into two groups of doubly degenerate E_u and three non-degenerate A_{2u} ($\times 2$) and A_{1u} ($\times 1$) components. The order of the ${}^2A_{1u}$ and 2E_u states is reversed in NaYbO₂ as compared to NaYbS₂.

Yb ³⁺ $4f^{13}$ CF states	NaYbS ₂		NaYbO ₂	
	CASSCF	MRCI	CASSCF	MRCI
${}^2A_{2u}$	0	0	0	0
2E_u	9	10	23	27
${}^2A_{1u}$	23	29	74	85
2E_u	31	36	68	78
${}^2A_{2u}$	40	47	106	121

are obtained for NaYbO₂.

The SO-MRCI excitation energies are in reasonable agreement with available experimental data. For NaYbS₂, only two intense peaks originating from on-site f - f transitions are observed in inelastic neutron scattering (INS), at 23 and 39 meV [11]. Additional information was obtained however by electron-spin resonance (ESR), i.e., a low-energy excitation at 17 meV [11]. These experimental results are in very good correspondence with our data. For NaYbO₂, three intense peaks at 35, 58, and 83 eV are found by INS [13], also in this case not far from our results. By ESR, the low-energy excitation comes at a smaller energy of about 27 meV [12]. The details provided by our calculations will motivate further analysis for understanding the discrepancies between different experimental techniques.

It is worth to mention that earlier quantum chemical investigations of $4f$ systems were mainly carried out at the CASSCF/CASPT2 (complete active space second-order perturbation theory) level [36–40]. Here we report results of variational MRCI calculations: unlike non-variational methods, the calculated energy is in this case always higher than the actual energy. The calculation starts by choosing a ‘trial’ wavefunction and any variations which lower its energy are necessarily making the approximate energy closer to the exact solution. The MRCI treatment shows significant corrections to the excitation energies (see Table II), percentagewise comparable to the corrections found in d -electron oxides [41, 42].

TABLE II. Yb³⁺ $4f^{13}$ electronic structure as obtained by SO-CASSCF and SO-MRCI, in NaYbS₂ and NaYbO₂. Units of meV and notations for trigonal symmetry are used^a. A gap of ~ 1 eV similar to the free-ion ${}^2F_{7/2}$ - ${}^2F_{5/2}$ splitting is clearly visible.

Yb ³⁺ $4f^{13}$ SO states	NaYbS ₂		NaYbO ₂	
	SO-CASSCF	SO-MRCI	SO-CASSCF	SO-MRCI
Γ_6	0	0	0	0
Γ_6	11	15	40	39
$\Gamma_4+\Gamma_5$	18	23	42	46
Γ_6	30	39	92	92
Γ_6	1277	1300	1320	1319
$\Gamma_4+\Gamma_5$	1282	1305	1324	1326
Γ_6	1300	1329	1383	1383

^a See, e.g., Table 14 in Appendix B of Ref. 35.

Cation charge imbalance effects

Overall, our calculations (see Table I) indicate a sizeable effect of trigonal distortions on the $4f$ multiplet structure, in both NaYbX₂ compounds. While for two-dimensional Yb³⁺ triangular-lattice systems such as NaYbS₂, NaYbO₂, and YbMgGaO₄, in the magnetic layer of Yb(O/S)₆ octahedra, the anion site is limited to a 2− ionic charge, in the non-magnetic layer(s) different substitution is possible [11–13, 16, 17]. In order to gain better insight into the effect of the nearby surroundings on the $4f$ -level splittings, we performed additional calculations for hypothetical MgYbX₂ systems. To this end, we replaced the inter-layer Na¹⁺ species by Mg²⁺ cations, in both delafossite structures, NaYbS₂ and NaYbO₂ [31, 32]. Embedding potentials for fictitious lattice configurations with 2+ cations at all metal sites (Yb- and A-ion positions) were constructed and CASSCF and MRCI computations similar to those already discussed above were performed. As we aim to maintain the reference-ion charge-state as Yb³⁺ within a lattice of Mg²⁺, Yb²⁺, and X^{2−} species, in order to keep overall charge neutrality, we added one negative charge within the nearby crystalline surroundings. Large-core pseudopotentials incorporating all occupied shells of the Mg ion were used [43]. For the six Yb²⁺ NN’s, we again applied large-core pseudopotentials that also incorporate the f shell [22].

Results for the Yb³⁺ f -level splittings as obtained by CASSCF and MRCI sans SOC are provided for the hypothetical MgYbS₂ and MgYbO₂ systems in Table III. In comparison with the ‘real’ Na-based compounds, the more homogeneous electrostatic surroundings in MgYbX₂ yield different CF splittings. In particular, the latter are modified in MgYbS₂ such that the ${}^2A_{2u}$ - 2E_u and ${}^2A_{1u}$ - 2E_u gaps are reduced to only ≈ 2 meV. This structure resembles now the $4f$ CF splittings in cubic symmetry, where the $4f$ levels are grouped into two sets of triply-degenerate T states and one non-degenerate A component [44]. It looks as the effect of trigonal compression of the ligand cage is here cancelled out by the effect of the anisotropic (i.e., layered) crystalline surroundings. In MgYbO₂, on the other hand, a close-to-cubic CF level diagram is not achieved. But this is not at all surprising, given the different bond-lengths (metal-X and metal-metal) and the different amount of trigonal compression (X-Yb-X angles) in the S-based and O-based systems.

SO-CASSCF and SO-MRCI results for MgYbX₂ are shown in Table IV. As in the Na-based compounds, the Γ_6 state remains the lowest SO state for these more symmetric lattices with 2+ cations species in place. The MRCI treatment brings again sizeable corrections to the CASSCF relative energies. As concerns the MRCI data, the lower four Kramers doublets are at 0, 15, 17, and

TABLE III. CASSCF and MRCI relative energies (meV) for the f -shell single-hole levels sans SOC for a hypothetical MgYbX₂ delafossite lattice of Mg²⁺ (replacing Na¹⁺), Yb²⁺, and X²⁻ ions, with a more homogenous cation charge distribution.

Yb ³⁺ 4 <i>f</i> ¹³ states sans SOC	MgYbS ₂		MgYbO ₂	
	CASSCF	MRCI	CASSCF	MRCI
² A _{2u}	0	0	0	0
² E _u	2	2	36	37
² A _{1u}	20	26	43	50
² E _u	23	28	101	106
² A _{2u}	32	41	126	134

33 meV in MgYbS₂. The $\Gamma_4 + \Gamma_5$ state is split away from the Γ_6 state by only 2 meV, pointing again to a close-to-cubic 4*f*-shell electronic structure since in cubic symmetry the free-ion $J = 7/2$ multiplet transforms into two Γ_6 , Γ_7 doublets and one Γ_8 quartet [35]. In MgYbO₂, the low-lying four Kramers doublets are obtained at relative energies of 0, 24, 64, and 100 meV, with significantly larger splittings.

Using the obtained SO wavefunctions we have also calculated the magnetic g tensors of all compounds, using the Gerloch-McMeeking formula [45]. The detailed computational scheme is described in Ref. 7. Ground-state g factors for all AYbX₂ (A = Na, Mg and X = S, O) systems are listed in Table V, alongside with available experimental data.

The MRCI g factors are $g_{ab} = 3.19$, $g_c = 0.93$ in NaYbS₂ and $g_{ab} = 3.31$, $g_c = 0.87$ in NaYbO₂, where

TABLE IV. Yb³⁺ f^{13} SO states for a more symmetric cation charge distribution as realized in MgYbX₂ (X = S, O), with 2+ charges at all surroundings cation sites. Units of meV are used.

Yb ³⁺ 4 <i>f</i> ¹³ SO states	MgYbS ₂		MgYbO ₂	
	SO-CASSCF	SO-MRCI	SO-CASSCF	SO-MRCI
Γ_6	0	0	0	0
Γ_6	11	15	22	24
$\Gamma_4 + \Gamma_5$	14	17	62	64
Γ_6	26	33	95	100
Γ_6	1279	1304	1279	1302
$\Gamma_4 + \Gamma_5$	1279	1305	1310	1331
Γ_6	1297	1328	1361	1386

the crystallographic c axis is perpendicular to the (ab) Yb honeycomb plane. Also according to ESR data [11], the g factors are highly anisotropic in NaYbS₂, in good agreement with our calculated g factors. On the other hand, in NaYbO₂, the g factor along the c axis is underestimated in our calculations with respect to the ESR measurements [12]. The exact reason of this discrepancy is still unclear; however, given the different estimations for the position of the first excited state by ESR, INS [11–13], and SO-MRCI, it was foreseeable to arrive to different g factors in the latter compound.

It is seen that the most isotropic g factors are computed in the MgYbS₂ system, namely $g_{ab} = 2.73$, $g_c = 2.49$ by SO-MRCI, and in MgYbO₂, $g_{ab} = 3.09$, $g_c = 3.25$. This again indicates that the MgYbS₂ potential is rather close to the cubic octahedral limit with $g_{ab}^{cub} = g_c^{cub} = 2.67$. The more isotropic structure of the g factors is dictated by the redistribution of positive charge around the magnetic center: the Yb center experiences a more homogeneous electrostatic environment with 2+ ionic charges at NN sites both in the inter-layer region and within the magnetic plane.

TABLE V. Ground-state g factors in AYbX₂ (A = Na, Mg and X = S, O) as obtained from SO-CASSCF and SO-MRCI. Results as found by ESR are also provided.

System	CASSCF		MRCI		Experiment	
	g_{ab}	g_c	g_{ab}	g_c	g_{ab}	g_c
NaYbS ₂	3.21	0.80	3.19	0.93	3.19	0.57
MgYbS ₂	2.73	2.49	2.73	2.49		
NaYbO ₂	3.82	1.01	3.31	0.87	3.28	1.75
MgYbO ₂	2.85	4.26	3.09	3.25		

Conclusions

To sum up, on the basis of the quantum chemical calculations, we provide a detailed analysis of the Yb³⁺ 4*f*¹³ electronic structure in NaYbS₂ and NaYbO₂. Significantly larger CF splittings are found in the latter, since the Yb-O bonds are shorter and the amount of trigonal distortion larger. The magnetic g factors extracted from these computations are highly anisotropic. In particular, we obtained larger g factors within the magnetic ab layer. It turns out that this single-site magnetic anisotropy is largely controlled by cation charge imbalance in the nearby surroundings. According to our data, with a more symmetric cation charge distribution around the reference octahedron, the f -level splittings of the paramagnetic center are modified to a quasi-cubic energy diagram and the g factors become more isotropic in both NaYbX₂ systems. The fact that in the sulphide especially the electronic structure brings back to

the high-symmetry case when using more homogeneous surrounding charges, even if the octahedron is distorted and the local symmetry is D_{3d} , indicates an interesting situation with near cancellation between the effect of trigonal compression of the ligand cage and the effect of having anisotropic (i.e., layered) longer-range surroundings. Our results suggest that the interplay of ligand-cage distortions, longer-range structural anisotropy, and cation charge imbalance in the immediate neighborhood provides means of varying the single-site g_c , g_{ab} factors over a rather broad range. More involved computations are required to determine how these knobs can be used for tuning the intersite magnetic couplings.

Acknowledgments

We acknowledge M. Baenitz, J. Sichelschmidt, A. Tsirlin, D. Inosov, Ph. Schlender, and K. Ranjith for inspiring discussions and U. Nitzsche for technical support. Z. Z., S. A., and L. H. acknowledge financial support from the German Research Foundation (Deutsche Forschungsgemeinschaft, DFG). This work was also supported by SFB1143 project A5 and the Würzburg-Dresden Cluster of Excellence ct.qmat.

Bibliography

-
- [1] J. B. Goodenough, "An interpretation of the magnetic properties of the perovskite-type mixed crystals $\text{La}_{1-x}\text{Sr}_x\text{CoO}_{3-\lambda}$," *J. Phys. Chem. Sol.* **6**, 287 – 297 (1958).
- [2] P. W. Anderson, "New approach to the theory of superexchange interactions," *Phys. Rev.* **115**, 2 – 13 (1959).
- [3] J. Kanamori, "Theory of the Magnetic Properties of Ferrous and Cobaltous Oxides, I," *Prog. Theor. Phys.* **17**, 177 – 196 (1957).
- [4] J. Kanamori, "Theory of the Magnetic Properties of Ferrous and Cobaltous Oxides, II," *Prog. Theor. Phys.* **17**, 197 (1957).
- [5] J. Kanamori, "Superexchange interaction and symmetry properties of electron orbitals," *J. Phys. Chem. Sol.* **10**, 87 – 98 (1959).
- [6] L. Xu, N. A. Bogdanov, A. Princep, P. Fulde, J. van den Brink, and L. Hozoi, "Covalency and vibronic couplings make a nonmagnetic $j = 3/2$ ion magnetic," *npj Quantum Mater.* **1**, 16029 (2016).
- [7] N. A. Bogdanov, V. M. Katukuri, J. Romhanyi, V. Yushankhai, V. Kataev, B. Büchner, J. van den Brink, and L. Hozoi, "Orbital reconstruction in nonpolar tetravalent transition-metal oxide layers," *Nat. Commun.* **6**, 7306 (2015).
- [8] R. Yadav, R. Ray, M. S. Eldeeb, S. Nishimoto, L. Hozoi, and J. van den Brink, "Strong Effect of Hydrogen Order on Magnetic Kitaev Interactions in $\text{H}_3\text{LiIr}_2\text{O}_6$," *Phys. Rev. Lett.* **121**, 197203 (2018).
- [9] R. Yadav, M. S. Eldeeb, R. Ray, S. Aswartham, M. I. Sturza, S. Nishimoto, J. van den Brink, and L. Hozoi, "Engineering Kitaev exchange in stacked iridate layers: impact of inter-layer species on in-plane magnetism," *Chem. Sci.* **10**, 1866 (2019).
- [10] N. A. Bogdanov, R. Maurice, I. Rousochatzakis, J. van den Brink, and L. Hozoi, "Magnetic State of Pyrochlore $\text{Cd}_2\text{Os}_2\text{O}_7$ Emerging from Strong Competition of Ligand Distortions and Longer-Range Crystalline Anisotropy," *Phys. Rev. Lett.* **110**, 127206 (2013).
- [11] M. Baenitz, Ph. Schlender, J. Sichelschmidt, Y. A. Onykiienko, Z. Zangeneh, K. M. Ranjith, R. Sarkar, L. Hozoi, H. C. Walker, J.-C. Orain, H. Yasuoka, J. van den Brink, H. H. Klauss, D. S. Inosov, and Th. Doert, "NaYbS₂: A planar spin-1/2 triangular-lattice magnet and putative spin liquid," *Phys. Rev. B* **98**, 220409(R) (2018).
- [12] K. M. Ranjith, D. Dmytriieva, S. Khim, J. Sichelschmidt, S. Luther, D. Ehlers, H. Yasuoka, J. Wosnitza, A. A. Tsirlin, H. Kühne, and M. Baenitz, "Field-induced instability of the quantum-spin-liquid ground state in the $J_{\text{eff}} = 1/2$ triangular-lattice compound NaYbO₂," *Phys. Rev. B* **99**, 180401(R) (2019).
- [13] L. Ding, M. Pascal, S. Bachus, F. Grubler, P. Gegenwart, J. Singleton, R. D. Johnson, H. C. Walker, D. T. Adroja, A. D. Hillier, and A. A. Tsirlin, "Gapless spin-liquid state in the structurally disorder-free triangular antiferromagnet NaYbO₂," *arXiv:1901.07810*.
- [14] W. Liu, Z. Zhang, J. Ji, Y. Liu, J. Li, H. Lei and Q. Zhang, "Rare-Earth Chalcogenides: A Large Family of Triangular Lattice Spin Liquid Candidates," *Chin. Phys. Lett.* **35**, 117501 (2018).
- [15] M. Bordelon, E. Kenney, T. Hogan, L. Posthuma, M. Kavand, Y. Lyu, M. Sherwin, C. Brown, M. J. Graf, L. Balents, and S. D. Wilson, "Field-tunable quantum disordered ground state in the triangular lattice antiferromagnet NaYbO₂," *arXiv:1901.09408*.
- [16] Y. Shen, Y.-D. Li, H. Wo, Y. Li, S. Shen, B. Pan, Q. Wang, H. C. Walker, P. Steffens, M. Boehm, Y. Hao, D. L. Quintero-Castro, L. W. Harriger, M. D. Frontzek, L. Hao, S. Meng, Q. Zhang, G. Chen, and J. Zhao, "Evidence for a spinon Fermi surface in a triangular-lattice quantum-spin-liquid candidate," *Nature (London)* **540**, 559 – 562 (2016).
- [17] Y. Li, H. Liao, Z. Zhang, S. Li, F. Jin, L. Ling, L. Zhang, Y. Zou, L. Pi, Z. Yang, J. Wang, Z. Wu, and Q. Zhang, "Gapless quantum spin liquid ground state in the two-dimensional spin-1/2 triangular antiferromagnet YbMgGaO₄," *Sci. Rep.* **5**, 16419 (2015).
- [18] Y. Li, G. Chen, W. Tong, L. Pi, J. Liu, Z. Yang, X. Wang, and Q. Zhang, "Rare-Earth Triangular Lattice Spin Liquid: A Single-Crystal Study of YbMgGaO₄," *Phys. Rev. Lett.* **115**, 167203 (2015).
- [19] Y.-D. Li, X. Wang, and G. Chen, "Anisotropic spin model of strong spin-orbit-coupled triangular antiferromagnets," *Phys. Rev. B* **94**, 035107 (2016).
- [20] J. A. M. Paddison, M. Daum, Z. Dun, G. Ehlers, Y. Liu, M. B. Stone, H. Zhou, and M. Mourigal, "Continuous excitations of the triangular-lattice quantum spin liquid YbMgGaO₄," *Nat. Phys.* **13**, 117 (2017).
- [21] Y. Li, D. Adroja, P. K. Biswas, P. J. Baker, Q. Zhang, J. Liu, A. A. Tsirlin, P. Gegenwart, and Q. Zhang, "Muon

- Spin Relaxation Evidence for the U(1) Quantum Spin-Liquid Ground State in the Triangular Antiferromagnet YbMgGaO₄,” *Phys. Rev. Lett.* **117**, 097201 (2016).
- [22] A. Savin, M. Dolg, H. Stoll and H. Preuss, “Energy-adjusted pseudopotentials for the rare earth elements,” *Theor. Chim. Acta* **75**, 173–194 (1989).
- [23] H. J. Werner, P. J. Knowles, G. Knizia, F. R. Manby, and M. Schütz, “Molpro: a general-purpose quantum chemistry program package,” *Wiley Rev: Comp. Mol. Sci.* **2**, 242–253 (2012).
- [24] T. Helgaker, P. Jørgensen, J. Olsen, *Molecular electronic-structure theory* (Wiley, Chichester, 2000).
- [25] M. Dolg, H. Stoll, and H. Preuss, “Energy adjusted *ab initio* pseudopotentials for the rare earth elements,” *J. Chem. Phys.* **90**, 1730 (1989).
- [26] X. Cao and M. Dolg, “Valence basis sets for relativistic energy-consistent small-core lanthanide pseudopotentials,” *J. Chem. Phys.* **115**, 7348 (2001).
- [27] X. Cao and M. Dolg, “Segmented contraction scheme for small-core lanthanide pseudopotential basis sets,” *J. Mol. Struct. (Theochem)* **581**, 139 (2002).
- [28] D. E. Woon and T. H. Dunning Jr., “Gaussian basis sets for use in correlated molecular calculations. III. The atoms aluminum through argon,” *J. Chem. Phys.* **98**, 1358 (1993).
- [29] T. H. Dunning, “Gaussian basis sets for use in correlated molecular calculations. I. The atoms boron through neon and hydrogen,” *J. Chem. Phys.* **90**, 1007 (1989).
- [30] P. Fuentealba, H. Preuss, H. Stoll, and L. v. Szentpaly, “A proper account of core-polarization with pseudopotentials: single valence-electron alkali compounds,” *Chem. Phys. Lett.* **89**, 418 (1982).
- [31] T. Schleid and F. Lissner, *Eur. J. Solid. State. Inorg. Chem.* **30**, 829 (1993).
- [32] Y. Hashimoto, M. Wakeshima, and Y. Hinatsu, “Magnetic properties of ternary sodium oxides NaLnO₂ (Ln = rare earths),” *J. Solid State Chem.* **176**, 266–272 (2003).
- [33] P. W. Atkins, M. S. Child, and C. S. G. Phillips, *Tables for Group Theory* (Oxford University Press, 1970).
- [34] A. Berning, M. Schweizer, H.-J. Werner, P. J. Knowles, and P. Palmieri, “Spin-orbit matrix elements for internally contracted multireference configuration interaction wavefunctions,” *Mol. Phys.* **98**, 1823–1833 (2000).
- [35] A. Abragam and B. Bleaney, “Electron Paramagnetic Resonance of Transition Ions,” (Oxford University Press, 1970).
- [36] L. Seijo and Z. Barandiaràn, “Large splittings of the 4*f* shell of Ce³⁺ in garnets,” *Phys. Chem. Chem. Phys.* **16**, 3830 (2014).
- [37] K. S. Pedersen, L. Ungur, M. Sigrist, A. Sundt, M. Schau-Magnussen, V. Vieru, H. Mutka, S. Rols, H. Weihe, O. Waldmann, L. F. Chibotaru, J. Bendix and J. Dreiser, “Modifying the properties of 4*f* single-ion magnets by peripheral ligand functionalisation,” *Chem. Sci.* **5**, 1650 (2014).
- [38] F. Gendron, B. Pritchard, H. Bolvin and J. Autschbach, “Single-ion 4*f* element magnetism: an *ab initio* look at Ln(COT)₂⁻,” *Dalton Trans.* **44**, 19886 (2015).
- [39] F. Aiga, R. Hiramatsu, K. Ishida, “*Ab initio* theoretical study of 4*f* → 5*d* transitions in Eu²⁺-doped CaF₂,” *J. Lumin.* **145**, 951 (2014).
- [40] L. Ning, L. Lin, L. Li, Ch. Wu, Ch. Duan, Y. Zhang and L. Seijo, “Electronic properties and 4*f* → 5*d* transitions in Ce-doped Lu₂SiO₅: a theoretical investigation,” *J. Mater. Chem.* **22**, 13723 (2012).
- [41] V. M. Katukuri, K. Roszeitis, V. Yushankhai, A. Mitrushchenkov, H. Stoll, M. van Veenendaal, P. Fulde, J. van den Brink, and L. Hozoi, “Electronic Structure of Low-Dimensional 4*d*⁵ Oxides: Interplay of Ligand Distortions, Overall Lattice Anisotropy, and Spin-Orbit Interactions,” *Inorg. Chem.* **53**, 4833 (2014).
- [42] H.-Y. Huang, N. A. Bogdanov, L. Siurakshina, P. Fulde, J. van den Brink, and L. Hozoi, “*Ab initio* calculation of *d-d* excitations in quasi-one-dimensional Cu *d*⁹ correlated materials,” *Phys. Rev. B* **84**, 235125 (2011).
- [43] P. Fuentealba, L. v. Szentpaly, H. Preuss, and H. Stoll, “Pseudopotential calculations for alkaline-earth atoms,” *J. Phys. B: At. Mol. Phys.* **18**, 1287–1296 (1985).
- [44] W. Li, G. Zhou and T. Mak, *Advanced Structural Inorganic Chemistry* (Oxford University Press, 2008).
- [45] H. Bolvin, “An alternative approach to the *g*-matrix: theory and applications.” *ChemPhysChem* **7**, 1575 (2006).